Journal of Applied Sciences and Nanotechnology

Journal homepage: jasn.uotechnology.edu.iq

Coke Decomposition Kinetic Model of Spent Hydrodesulfurization Catalysts

Aymen F. Zween*, Zaidoon M. Shakor, Bashir Y. Sherhan

Department of Chemical Engineering, University of Technology - Iraq, Iraq

A R T I C L E I N F O

Article history:
Received: July, 20, 2024
Accepted: October, 19, 2024
Available online: December, 14, 2024

Keywords:
Hydrodesulfurization,
Bentonite,
Kaolin,
Catalyst,
Model

Corresponding Author:
Aymen F. Zween
aymenpetro81@gmail.com

A B S T R A C T

Recycling residue hydrodesulfurization (HDS) catalysts is essential due to frequent deactivation. Petroleum coke's high ignition temperature and complex combustion behavior stem from its graphite-like structure and low volatile matter. This study investigates petroleum coke combustion and oxidation kinetics with metal catalysts. Data from HDS catalysts (5% Co-10% Mo/active kaolin and 5% Co-10% Mo/active bentonite) are crucial for industrial regenerator simulations. Iraqi mineral clays, treated and loaded with cobalt and molybdenum, were used in HDS reactions of Iraqi gas oil with 10200 ppm sulfur at 360°C, 12 bar, and WHSV of 2 h^{-1}. Spent catalysts, coated with coke, were analyzed, and coke was removed using thermogravimetric analysis (TGA) at heating rates of 2.5, 5, and 10°C/min. MATLAB software assessed coke accumulation's impact on combustion activation energy via model-free and model-based methods. Activation energies for coke combustion were 46.48, 87.71, and 102.68 kJ/mol for hydrocarbons, soft coke, and hard coke, respectively, on 5% Co-10% Mo/active kaolin, and 41.98, 68.11, and 100.38 kJ/mol for 5% Co-10% Mo/active bentonite. TGA revealed 7.553% and 7.977% total weight loss in kaolin and bentonite catalysts. The model-based method was most effective for regenerating aged HDS catalysts at 850°C, especially for hard coke removal. DTG analysis showed two concavities, indicating soft coke below 350°C and hard coke between 350 and 850°C. For 5%Co-10%Mo/kaolin catalysts, peak temperatures (T_{peak}) were 517, 526, and 610°C at heating rates of 2.5, 5, and 10°C/min. Bentonite catalysts showed lower T_{peak} values.

https://doi.org/10.53293/jasn.2024.7465.1305, Department of Applied Sciences, University of Technology - Iraq.
© 2024 The Author(s). This is an open access article under the CC BY license (http://creativecommons.org/licenses/by/4.0/).

1. Introduction

Natural petroleum resources, first exploited in the 19th century, have supplied the affordable energy needed for the recent unprecedented development in human society. It is no exaggeration to state that daily life depends completely on petroleum products. Petroleum is a mixture of hydrocarbons with many structures and molecular weights. In addition, petroleum contains many molecules that include heteroatoms such as sulfur, nitrogen and vanadium [1]. Petroleum coke (pet-coke) production, a secondary product of petroleum refining, has been rising alongside the increasing production of petroleum derivatives. Additionally, the increase in heavy oil refining has led to a higher yield of petroleum coke per refining unit [2, 3]. Many methods have been developed for

desulfurizing petroleum such as doctor treatment, copper sweetening and others. However, the HDS process is the most effective and feasible method, because sulfur is removed as H_2S just by contacting sulfur-containing compounds with a catalyst under a hydrogen atmosphere [1]. HDS was initially intended to reduce process corrosion [4], eliminate the sour odour called skunk juice [1], or improve the efficiency of tetra-alkyl lead used as an octane number booster for the gasoline fraction [5].

However, a new use of HDS was recognized in the 1960s, as public awareness of serious human health problems due to sulfur in petroleum was increased. The rapidly increasing consumption of petroleum-based on postwar rehabilitation and high economic growth in Japan significantly increased the number of patients with bronchial asthma and chronic bronchitis around industrial areas. Research has shown that SO_x emissions from petroleum are the most significant contributor, and the accumulation of coke on the catalyst is the main reason for catalyst deactivation in industrial catalytic reactors, leading to unstable operation of these units, therefore catalyst regeneration is crucial for these industrial operations [6]. A variety of HDS catalysts are currently employed in the oil industry, each designed to suit specific feed properties and reaction conditions [7].

The most commonly employed catalyst used in HDS, Co-Mo on active support, referred to as (CoMo) after a sulfidation step [8]. The conventional method for regenerating HDS catalysts involves an optimized thermal treatment that remains below 900 °C to reduce the formation of crystallized species, including $CoMoO_4$ or $CoAl_2O_4$. This regeneration process is effective in restoring catalytic activity, which reaches around 90% of the original performance [9]. Many excellent reviews and articles on HDS have been published since the early 1950s [10-13]. Interestingly, the origin of HDS catalysts is rarely discussed. One possible reason is that HDS catalyst technologies have primarily been developed by industrial companies, and the history of their development may involve commercial secrets. However, the origin of HDS catalysts is of great interest to all HDS catalyst researchers. This origin can be traced back to experimental studies conducted in the early 20th century [14]. In particular, the important studies on the hydrogenation of coal and heavy oil under high pressure by Friedrich Bergius and Carl Bosch in Germany during the 1910s [15].

Considering that petroleum coke predominantly has a structure similar to graphite, it is reasonable to suggest that catalysts effective in oxidizing graphite could also be tested for combustion of petroleum coke. Additionally, studies on the oxidation processes of various carbon-rich substances, like soot, suggest that catalysts that utilize transition-metal oxides as well as lanthanides for instance iron, copper, and cerium oxides show substantial catalytic activity, making them highly effective in various chemical processes [16]. Alongside oxides, Noteworthy is the fact that transition-metal chlorides demonstrate exceptional catalytic activity in the oxidation of carbon-rich materials [17, 18]. ‘Thermogravimetric analysis (TGA) is typically employed to analyze the burning process and measure the kinetic constants in solid fuels, including petroleum coke as well as coal [19-24].

Moreover, TGA experiments are straightforward and efficient, and when accompanied by appropriate data handling, they can provide exact kinetic measurements. Various techniques which have been applied to analyze kinetic data for solid-state processes obtained from TGA are generally categorized within model-fitting as well as model-free methods. The model-free approach requires multiple reaction rate curves, deriving kinetic parameters for identical degrees of conversion derived from the plots obtained at various heating rates. Conversely, the model-fitting method explores different models to fit the data, using algebraic functions to link experimental data with theoretical models for reaction kinetics, thus reflecting the interplay between reaction rate as well as conversion extent, and correlating it to the reaction pathway. The model that most accurately represents the data is selected for kinetic analysis and parameter determination.

Consequently, model-fitting approaches are routinely employed to extract activation energy and the Arrhenius constant from a single TGA measurement set [25]. Many studies have utilized diverse experimental conditions for TGA for plastics pyrolysis reactions, including a variety of heating rates as well as sample masses, temperature, and reaction process atmospheres [26-32]. To understand the various techniques for model treatment used to determine Arrhenius-based kinetic metrics in the pyrolysis process often observed through TGA a review of past research has been conducted as outlined below:

Shakor Z. *et al*., [33] determined activation energy (Ea) for the coke-pyrolysis accumulated on utilized hydrocracking and reforming catalysts using a reaction-based model and the traditional model-free method. The theoretical results from the multi-reaction model for coke decomposition are consistent with the experimental results for both catalysts. Pajri S. *et al*. [34] employed TGA in the presence of air to quantify coke deposition and determine the coke-burning kinetic parameters. They utilized certain models (non-isothermal ways): (Friedman, Flynn-Wall-Ozawa (FWO), as well as Kissinger-Akahira-Sunose (KAS)) to ascertain the energy of activation and identify the optimal model fitting their empirical findings. The FWO method exhibited the optimum fit for $3Pt/Al_2O_3$ as well as $3Pt\text{-}0.5Sn/Al_2O_3$, while all these models yielded equivalent fits for $3Pt\text{-}1Sn/Al_2O_3$, $3Pt\text{-}2Sn/Al_2O_3$, and $3Pt\text{-}3Sn/Al_2O_3$. Fan H. *et al*. [35] employed both model-fit which is based on nonlinear equation style and model-free which is based on linear equations to investigate the parameters from the oxidation process of coal char. Their findings indicated that the model based on random pores provided the most accurate correlation with experimental data. Under best conditions in MA and MO atmospheres, the activation energies for coal char were significantly higher (103.2 kJ/mol and 97.3 kJ/mol, respectively) compared to conventional methods. Guodong J. and Liping W. [36] identified a suitable model for describing coal pyrolysis using Zhundong coal as a case study. They applied four iso-conversional kinetic methods—FWO, and KAS—to fit TGA data. Analysis of Arrhenius constant factors and values of activation energy as results from various models indicated that the FWO model provided the most accurate description of Zhundong coal pyrolysis. Leroy V. *et al*. [37] investigated the kinetics of forest fuel thermal decomposition using thermogravimetry under air and non-isothermal conditions ranging from 400 to 900 K. They utilized the classical model-free KAS method to calculate the energy of reaction activation energy as a function of reaction conversion across the entire temperature range. Their results demonstrated strong agreement between experimental data and simulations, validating their proposed approach. Alhulaybi Z. and Ibrahim D. [38] Studied the Comprehensive Kinetic of PET Pyrolysis Using TGA Data, where provided a detailed kinetic analysis of polyethene terephthalate (PET) pyrolysis using TGA data, applying multiple model-free methods such as the Friedman, FWO, and KAS methods were fitted to the experimental data to obtain the Ea and Ao of the reaction kinetics.

In this investigation, TGA data were employed to analyze the spent catalyst previously utilized in the HDS of gas oil. The TGA data was employed to apply both model-free and model-based kinetic models, marking the first time and new approach these methods have been applied to this specific type of catalyst. The literature review highlighted several key studies that have successfully employed these kinetic models, demonstrating their reliability and accuracy. For instance, model-free methods, such as the KAS and FWO methods, as well as model-based methods, were shown to provide results that closely matched experimental data in various applications. By employing both model-free and model-based methods, this research aims to validate these approaches' effectiveness in analyzing the spent HDS catalysts.

The study is expected to show exceptional results that have not been previously achieved by any research for this type of catalyst used in HDS reactions, as most previous studies used TGA models of catalysts for cracking or isomerization reactions. A key distinction in our research is that the coke deposition on the catalyst was specifically achieved through its use in the desulfurization of Iraqi gas oil in the presence of hydrogen under certain conditions. This unique approach highlights the relevance and specificity of our findings. Thereby, reinforcing the utility of these kinetic models in catalyst analysis. This validation will demonstrate that these methods are not only appropriate but also advantageous for use in similar research, providing a strong basis for their application in the investigation of utilized HDS catalysts.

2. Materials and Methods

2.1 Materials

The local mineral clays, consisting of Kaolin ($Al_2Si_2O_4(OH)_4$) and Bentonite ($Al_2H_2O_6Si$) were provided by the Iraqi Geological Survey along with their chemical analysis, which is listed in Table 1. The remaining materials used in the study were sodium hydroxide (NaOH, 98%), ammonium chloride (NH_4Cl, 99.9%), Polyvinyl Alcohol (99%), cobalt (II) nitrate ($Co(NO_3)_2.6H_2O$, 98%), and ammonium molybdate ($(NH4)_6MO_7O_{24}.4H_2O$, 99.98%). These materials were obtained from reputable chemical companies, namely Merck and Sigma Aldrich, and used in their original form. The De-ionized water (DI) was sourced from the local market.

Table 1: Chemical analysis of local clays.

Bentonite Clay		Kaolin Clay	
Component	**Weight %**	**Component**	**Weight %**
SiO_2	52.60	**SiO_2**	53.21
Al_2O_3	30.24	**Al_2O_3**	32.13
Fe_2O_3	9.07	**Fe_2O_3**	1.41
K_2O	0.5	**K_2O**	0.35
Na_2O	1.10	**Na_2O**	0.21
MgO	2.78	**MgO**	0.13
CaO	3.49	**CaO**	0.15
Cl	0.40	**TiO_2**	0.41
***L.O.I**	0.38	***L.O.I**	12.00
SO3	0.34	*L.O.I = Loss on Ignition	

These clays were chosen due to their cost-effectiveness. They were treated and then loaded with cobalt and molybdenum according to Fig.1 below. The catalyst powder was mixed with a 5% solution of polyvinyl alcohol (PVA) to create a paste. This paste was pressed under high pressure to form tablets of a specific size. The tablets were then ground and sieved to obtain catalyst pellets within the desired size range. Finally, the pellets were carefully packed into the reactor to prevent any pressure drop during the HDS reactions.

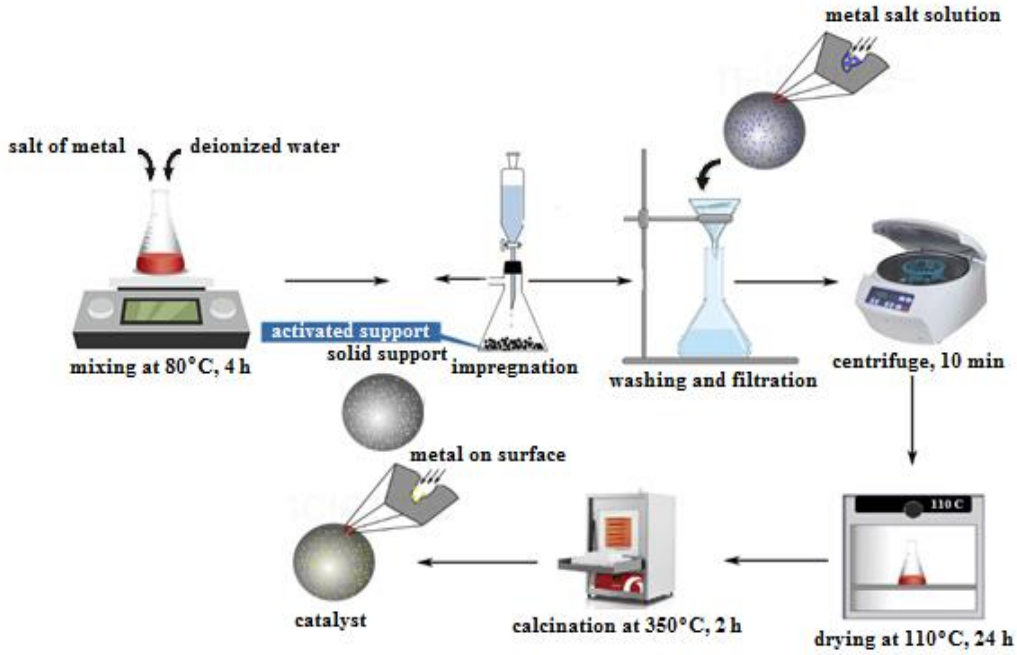

Figure 1: The schematic diagram for the metal loading procedure on the catalyst surface.

2.2 Catalyst Activity

The hydro-desulfurization catalytic activity evaluation was conducted using a high-pressure reactor unit (12 bar) and 360 °C temp. with a constant H_2/C ratio of 50 cm^3/cm^3 and an WHSV of 2 h^{-1}. Catalyst pellets of size around 4000 µm were packed into the reactor (with specific dimensions (12.4 mm diameter and 51 cm length)) in two layers. Iraqi gas oil and hydrogen gas were introduced into the reactor under controlled conditions. After the reaction, the product was separated into gaseous and liquid components. The liquid product was sampled and allowed to settle for 24 hours. Fig. 2 of the flow diagram displayed all of these stages.

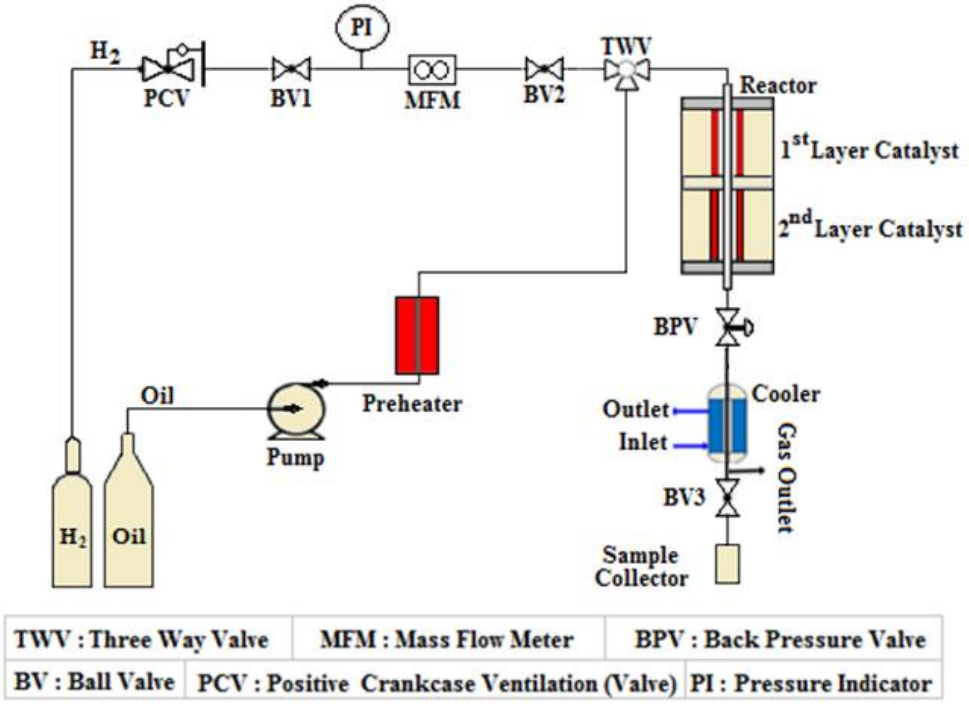

Figure 2: Scheme of the Experimental Setup of the HDS Unit.

2.3 Catalyst Regeneration

After concluding the reaction, the catalyst extraction is then analyzed through a TGA test. This test identifies the suitable temperature for reactivation, ensuring precise combustion of accumulated coke, and determines the optimal rate of temperature increase per minute.

2.4 Methods

The study employed Thermal Gravimetric Analysis/Differential Thermal Gravimetry (TGA-DTG) using a TA Q600-SDT Version 20.9-Build 20.0 device to investigate the thermal decomposing of spent catalysts. This was conducted under an inert nitrogen (N_2) atmosphere with the rate value of flow at 20 mL/min to prevent any reactions involving volatile emissions during the degradation of the substance. The temperature gradually increased starting with room atmosphere temperature (25 °C) to approximately 850 °C.

Throughout the experiments, strict control was maintained over particle size, initial sample weight (ranging from 0.9 to 1.2 g), and the N_2 flow rate. Detailed measurements of weight changes over time and temperature (TGA data) and their derivatives concerning temperature (DTG data) were continuously recorded and analyzed. Additionally, MATLAB software was utilized for the precise calculation of kinetic parameters, providing deeper insights into the decoking process of the catalysts.

2.4.1 Kinetic Modelling

The kinetics of coke material oxidation for the deactivated catalysts can be determined using the kinetic model related to the mass degradation rate [39]. The fundamental rate of mass loss equation applied in all kinetic studies is represented by Eq. (1) [40, 41].

$$\frac{d\alpha}{dt} = k(T)f(\alpha) \qquad (1)$$

Where the function k(T) serves as the reaction model, as well as k, is recognized as the decomposition rate kinetic constant. For every selected reaction mechanism, the rate coefficients are estimated across multiple temperatures using the Arrhenius equation [42], as described in Eq. (2) [40, 41]. The conversion degree α describes the decomposed quantity of the catalyst at time t, represented as elaborated by Eq. (3) [40, 41].

$$k(T) = A_0 e^{-E_a/RT} \quad (2)$$

$$\alpha = \frac{m_i - m_a}{m_i - m_f} \quad (3)$$

Where ma, mi, and mf designate the actual, initial, and final mass of the sample during the experiments, respectively. K(T) is substituted in Eq. (1) to derive Eq. (4) [40, 41]. Consequently, the temperature profile is a function that varies with time and is raised with a steady heating rate of β. The subsequent expression is calculated by Eq. (5) [40].

$$\frac{d\alpha}{dt} = A_0 f(\alpha) e^{-E_a/RT} \quad (4)$$

$$T = \beta t + T_o \quad (5)$$

where T0 denotes the starting temperature, β is the linear heating ramping rate, and T is the temperature at time t. For the non-isothermal method, TGA experiments are performed with a linear heating rate β, as described by Eq. (6) and (7) [40, 41]:

$$\beta = \frac{dT}{dt} \quad (6)$$

$$\frac{d\alpha}{dT}\frac{dT}{dt} = A_0 f(\alpha) e^{-E_a/RT} \quad (7)$$

Eq. (6) is substituted into Eq. (7) to derive Eq. (8) [40, 41]. Ea, R, K(T), and f(α) are determined using the reaction model to evaluate the activation energy (J.mol^{-1}). Eq. (8) is the result of the differential equation of the kinetic equation, which is applied during the approximation of kinetic analysis of the model-based method on differential simulation form.

$$\frac{d\alpha}{dT} = \frac{A_0}{\beta} f(\alpha) e^{-E_a/RT} \quad (8)$$

2.4.1.1 Model-Free Method

The model-free method, known as the 'iso-conversational method', is utilized to calculate the activation energy for various constant extents of coke conversion without considering specific arrangements as used in the reaction model [43]. The model-free method encompasses multi-curve methods, necessitating multiple kinetic curves for analysis [44]. Varying decomposition rates of the heating process were applied to calculate the activation energy and rate constant at specific conversions. A model-free approach was used to evaluate kinetic parameters without evaluating any reaction rate model for different constant rate extents of conversion [45]. The model-free techniques, such as FWO [46], KAS [47], Tang [48], and Starink [49] methods, were utilized for coke deactivation of spent catalyst to integrate the activation energy through the degree of conversion α. The linear form of four model-free techniques is listed in Table 2 to derive a linear plot between 1/T versus the left term of the equation to determine slope Ea/R and evaluate the activation energy Ea.

Table 2: Typical linear equation using model-free kinetic models [50-53].

Method	Model
FWO	$\ln\beta = \ln\left[\frac{AE_a}{Rg(\alpha)}\right] - 5.331 - 1.052\frac{E_a}{RT}$
KAS	$\ln\left(\frac{\beta}{T^2}\right) = \ln\left[\frac{AR}{E_a g(\alpha)}\right] - \frac{E_a}{RT}$
Tang	$\ln\left(\frac{\beta}{T^{1.894661}}\right) = \ln\left[\frac{AR^{0.92}}{g(\alpha)}\left(\frac{E_a}{R}\right)^{-0.894661}\right] - 0.37773896 - 1.00145033\frac{E_a}{RT}$
Starink	$\ln\left(\frac{\beta}{T^{1.92}}\right) = \ln\left[\frac{AR^{0.92}}{E_a{}^{0.92} g(\alpha)}\right] - 0.312 - 1.0008\frac{E_a}{RT}$

2.4.1.2 Model-Fitting Method of Reaction Model

The reaction model (model-fitting) method represented by the kinetic function is estimated by rigorously fitting the experimental data using advanced mathematical models obtained at a constant heating rate [54]. This approach enables the activation of a unified activation energy parameter encompassing the entire reaction process, estimating the complexity of solid-state reactions. Various expressions represent the transmutation function f(α) for the 'solid-state' reactions [55]. Table 3 lists the model-fitting-based methods for coke deactivation, covering nucleation, geometric shrinkage, diffusion, as well as reaction order frameworks, which were utilized to determine the correlation coefficient at different heating rates [56]. Eq. (9) represents the decomposition of materials with a narrow range of coke decomposition temperatures. For coke material with an extensive variety of decomposition components, multiple fit models can be applied to integrate the rate of decompositions (Eq. (10), where the total decomposition equals the sum of the individual material decomposition [57].

$$\alpha = \sum_i^n \alpha_i \qquad (9)$$

$$\frac{d\alpha_i}{dT} = \frac{A_i}{\beta} f(T) \mathrm{e}^{-E_i/RT} \qquad (10)$$

Table 3: Solid-state kinetics reaction models [52, 53].

	Reaction-Models		Differential form, f(α)	Integral form, g(α)
Nucleation Models	Power Law	P_2	$2\alpha^{1/2}$	$\alpha^{1/2}$
	Power Law	P_3	$3\alpha^{2/3}$	$\alpha^{1/3}$
	Power Law	P_4	$4\alpha^{3/4}$	$\alpha^{1/4}$
	Avreami-Erofeev	A_2	$2(1-\alpha)[-\ln(1-\alpha)]^{1/2}$	$[-\ln(1-\alpha)]^{1/2}$
	Avreami-Erofeev	A_3	$3(1-\alpha)[-\ln(1-\alpha)]^{2/3}$	$[-\ln(1-\alpha)]^{1/3}$
	Avreami-Erofeev	A_4	$4(1-\alpha)[-\ln(1-\alpha)]^{3/4}$	$[-\ln(1-\alpha)]^{1/4}$
	Modified Prout-Tompkins	B_1	$\alpha(1-\alpha)$	$\ln[\alpha/(1-\alpha)]$
Geometrical Contraction Models	Contructing cylinder	R_2	$2(1-\alpha)^{1/2}$	$1-(1-\alpha)^{1/2}$
	Contracting Sphere	R_3	$3(1-\alpha)^{2/3}$	$1-(1-\alpha)^{1/3}$
Diffusion Models	One-dimensional Diffusion	D_1	$1/2\alpha^{-1}$	α^2
	Two-dimensional Diffusion	D_2	$(-\ln(1-\alpha))^{-1}$	$(1-\alpha)*\ln(1-\alpha)+\alpha$
	3D-Diffusion control (Janders)	D_3	$3(1-\alpha)^{2/3}/[2(1-(1-\alpha)^{1/3})]$	$[1-(1-\alpha)^{1/3}]^2$
	Ginztling-Broanshtein	D_4	$3/[2((1-\alpha)^{-1/3}-1)]$	$1-(2/3)\alpha-(1-\alpha)^{2/3}$
Reaction Order Models	Mambel (First order)	F_1	$1-\alpha$	$-\ln(1-\alpha)$
	Second Order	F_2	$(1-\alpha)^2$	$(1-\alpha)^{-1}-1$
	Third Order	F_3	$(1-\alpha)^3$	$0.5((1-\alpha)^{-2}-1)$
	n-order reaction	F_n	$(1-\alpha)^n$	$1-(1-\alpha)^{1-n}/1-n$

2.5 Statistical Analysis

The Arrhenius's constant (Ao) and activation energy (Ea) of kinetic analysis were obtained through a fitting approach lessening the error between the model prediction and experimental data. The stochastic optimization method was implemented using MATLAB R2020a software. At each iteration, the conversion of mass loss of soft and hard coke oxidation was recalculated as a temperature-dependent function, with varying values of Ea and Ao to integrate the best-fit mechanism function. For both types of models, Eq. (11) [40] was employed to estimate the correlation coefficient (R^2), evaluating the model's efficacy formulated in this research. In this equation, (N) represents the experiment number, and the subscripts (exp.) and (pred.) indicate the experimental and forecasted findings of theoretical integration.

$$R^2 = 1 - \frac{\sum_{i=1}^{N}(y_{exp,i} - y_{pred,i})^2}{\sum_{i=1}^{N}(y_{exp,i} - \bar{y}_{exp})^2} \quad (11)$$

3. Experimental Procedure

3.1 Energy Dispersive X-Ray Analysis (EDX)

The elemental composition of various samples, including raw clays, activated clays, and activated clays loaded with different percentages of cobalt and molybdenum metals (5% and 10%) were analyzed using EDX as shown in Table 4. Additionally, the regenerated catalyst was examined to ensure that the metal ratios were maintained as shown in Tables 5 and 6. Primary components observed in the clays were oxygen, silicon, and aluminum, which contribute to their mildly acidic nature, as previously confirmed in the published literature [58]. Trace amounts of magnesium and other elements were also detected. Bentonite clay exhibited the presence of calcium and iron, while kaolin clay contained certain amounts of sodium. Upon treatment with ammonium chloride for clay activation, the exchangeable cations in both clays were effectively removed and replaced with acidic sites, specifically hydrogen groups (H-group). Overall, upon examining all the clays after the impregnation process, it can be concluded that the loading of cobalt and molybdenum metals was achieved successfully in the desired percentages.

Table 4: EDX results of catalyst clay samples.

	Substance	Raw	Activated	5% Co	10% Co	5% Mo	10% Mo	5% Co-10% Mo
Kaolin	Si	30.14	44.80	42.21	36.79	35.18	39.08	39.08
	Al	14.88	33.55	18.35	24.09	26.90	23.72	17.72
	Na	5.32	0.72	-	-	-	-	-
	O	46.76	20.85	34.32	28.11	32.35	26.24	26.57
	Co	-	-	4.90	10.93	-	-	5.20
	Mo	-	-	-	-	5.18	9.72	10.53
	Others	2.9	0.08	0.22	0.08	0.39	1.24	0.9
Bentonite	Si	31.29	29.80	39.46	35.39	38.20	35.20	30.92
	Al	11.45	14.98	19.28	23.92	31.72	25.02	22.76
	Na	3.71	0.53	-	-	-	-	-
	O	49.33	52.38	32.73	28.40	24.11	29.11	29.23
	Co	-	-	5.23	10.27	-	-	5.54
	Mo	-	-	-	-	5.09	9.75	10.21
	Others	4.22	2.31	3.3	2.02	0.88	0.92	1.34

Similarly, the EDX data revealed nearly identical outcomes in the quantity of metals present on the catalyst's surface both before and after the regeneration process. The weight ratio of Mo and Co was approximately 10.53 wt% and 5.2 wt% for the 5%Co-10%Mo/AK catalyst, and approximately 10.21 wt% and 5.54 wt% for the 5%Co-10%Mo/AB catalyst. Following the third regeneration, these ratios decreased by 6.8% and 4.4% for Mo and Co on activated kaolin, and by 3.7% and 0.54% for Mo and Co on activated bentonite. Tables 5 and 6 refer to these metal ratios and their diminishing quantities after each regeneration process.

Table 5: Percentages of Active Metals for 5%Co-10%Mo/Activated kaolin.

Active Phase Ratios				
Metal	**Original**	**After 1st Regeneration**	**After 2nd Regeneration**	**After 3rd Regeneration**
Mo	10.53	9.82	9.80	9.80
Co	5.21	5.09	5.02	4.98

Table 6: Percentages of Active Metals for 5%Co-10%Mo/Activated Bentonite.

Active Phase Ratios				
Metal	**Original**	**After 1st Regeneration**	**After 2nd Regeneration**	**After 3rd Regeneration**
Mo	10.21	9.88	9.84	9.82
Co	5.54	5.54	5.53	5.51

3.2 TGA, DTG and Models Results

The pet-coke weight reduction process at heating rates of varying magnitudes of 2.5, 5, and 10 °C/min and its differential thermogravimetry curves were demonstrated in Fig. 4 and 6 for HDS reaction by using optimum catalysts (5%Co-10%Mo/AK or AB). Accordingly, it can be recognized that increasing the heating rate can shift the behavior of the conversion curve.

It was noted there are two concavities or inflection points that are attributed to the presence of two reactions. Two types of coke were recognized on the catalyst, the first one is soft coke under 350 ºC and the second one is hard coke from 350 to 850 ºC. The table shows the reliance of the temperature on the heating rates of maximum removal rate for soft and hard coke, as indicated by the DTA peaks. As the heating rate was elevated, the temperature at which the coke decomposed at its maximum rate shifted upward. The maximum rate of coke decomposition of 5%Co-10%Mo/AB catalyst is higher than that for 5%Co-10%Mo/AK catalyst, and this can be attributed to the nature of bentonite clay in terms of its components, in addition to the ability of this catalyst to accumulate carbon on its surface and within its pores more than another catalyst. Moreover, the location of the catalyst in the lower layer of the reactor to remove complex sulfur compounds that the upper catalyst could not remove makes it more susceptible to spending and exposure to carbon amounts, especially hard carbon. By observing the curves and the tables, the effect can be observed the heating rate significantly impacted the peak value, inflexion point position and decomposition rate maximum. For the 5%Co-10%Mo/AK utilized catalyst, the peak temperatures (T_{peak}) were 517, 526 and 610 °C when the heating rates were 2.5, 5, and 10 °C/min, in the order given. This is attributed to the transmission constraints of the heat and mass in the amorphous carbon with graphitic coke and sulfide in a sample, which resulted in the differential in the inside and surface temperatures. While for the 5%Co-10%Mo/AB spent catalyst, the peak temperatures (T_{peak}) were shifted lower than the previously used catalyst due to the lower temperature of amorphous carbon with graphitic coke.

Table 7: Peak temperatures for heating rate.

Catalyst	Heating Rate	TPeak (°C)	$(d \propto)/dt$
5%Co-10%Mo/AK	2.5 °C/min	517	0.0212
	5 °C/min	526	0.0226
	10 °C/min	610	0.0237
5%Co-10%Mo/AB	2.5 °C/min	467	0.0251
	5 °C/min	525	0.0266
	10 °C/min	540	0.0387

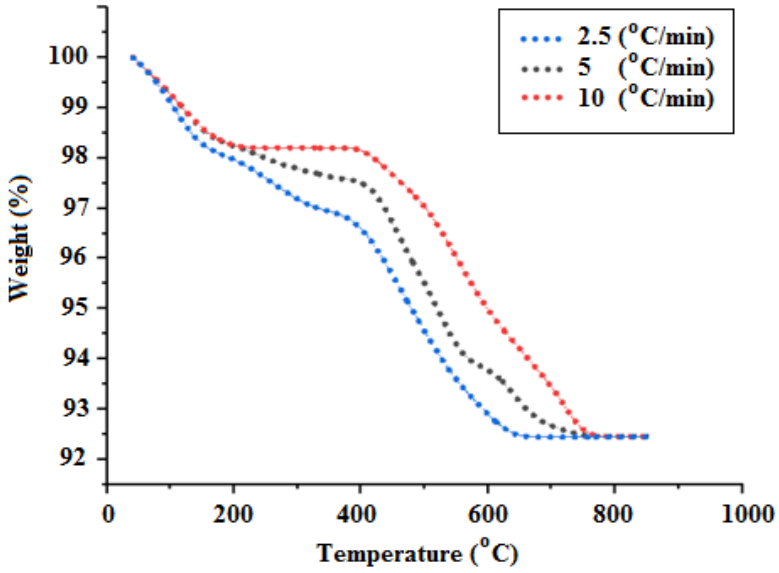

Figure 3: TGA curves at varying heating rate for 5%Co-10%Mo/AK catalyst.

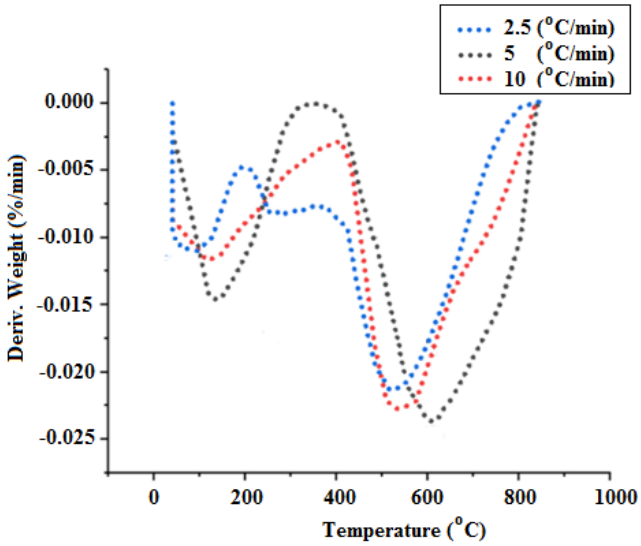

Figure 4: DTG curves at varying heating rate of 5%Co-10%Mo/AK catalyst.

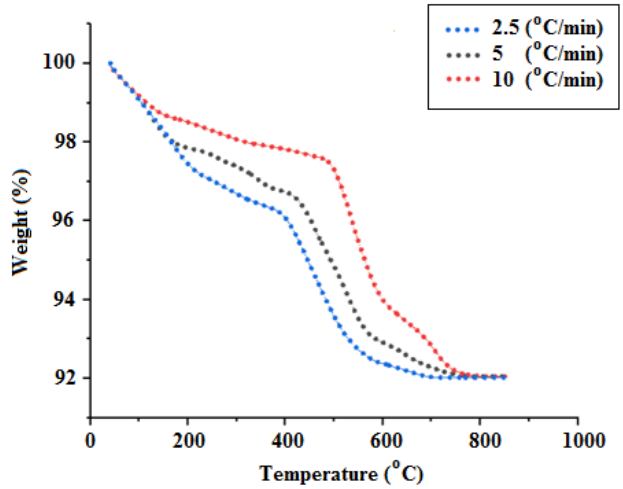

Figure 5: TGA curves at varying heating rate of 5%Co-10%Mo/AB catalyst.

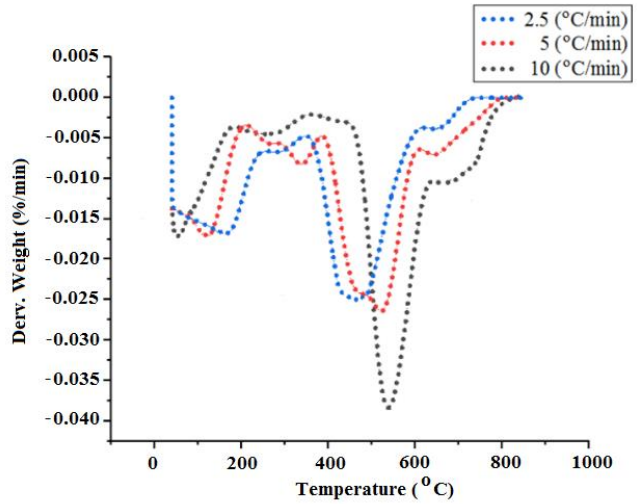

Figure 6: DTG curves at varying heating rate for 5%Co-10%Mo/AB catalyst.

3.3 Evaluation of Kinetic Parameters

3.3.1 Model-Free Method

This study compares four approaches free of model assumptions, inclusive FWO, KAS, Tang and Starink models, to analyze the non-isothermal kinetic analysis. Additionally, the thermal behavior of coke was determined to be over 5%Co-10%Mo/AK or AB-used catalysts. Fig. 7, 8, 9, and 10 represent linear plots from equations at different heating rates for FWO, KAS, Tang and Starink methods, respectively.

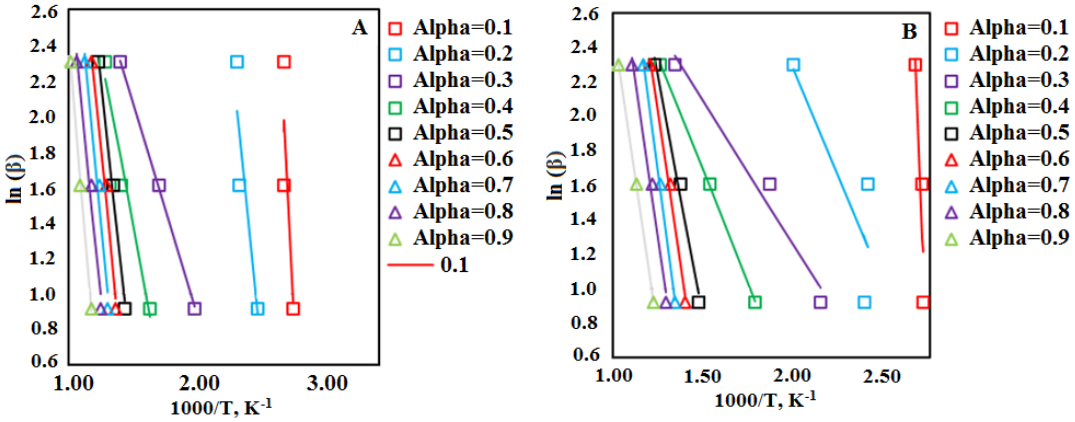

Figure 7: Linear regression lines of Flynn-Wall-Ozawa FWO method: [A] coke of spent 5%Co-10%Mo/AK catalyst, [B] coke of spent 5%Co-10%Mo/AB catalyst.

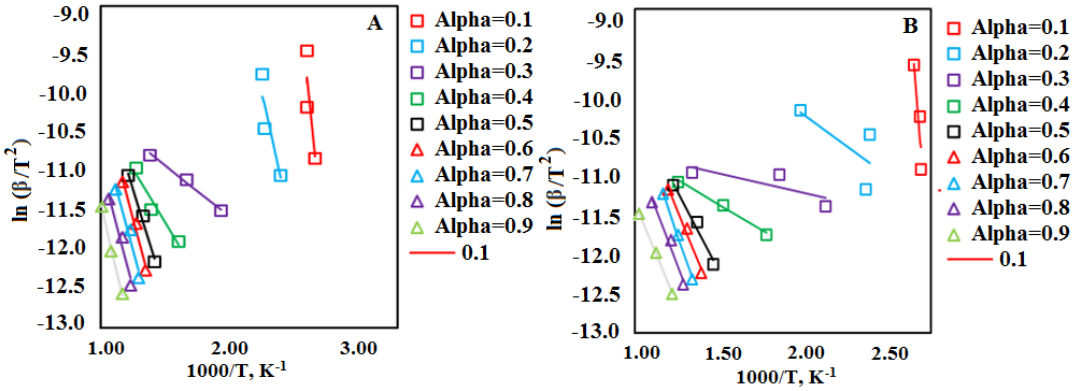

Figure 8: Linear regression lines of the KAS model at various conversion levels: [A] coke of spent 5%Co-10%Mo/AK catalyst, [B] coke of spent 5%Co-10%Mo/AB catalyst.

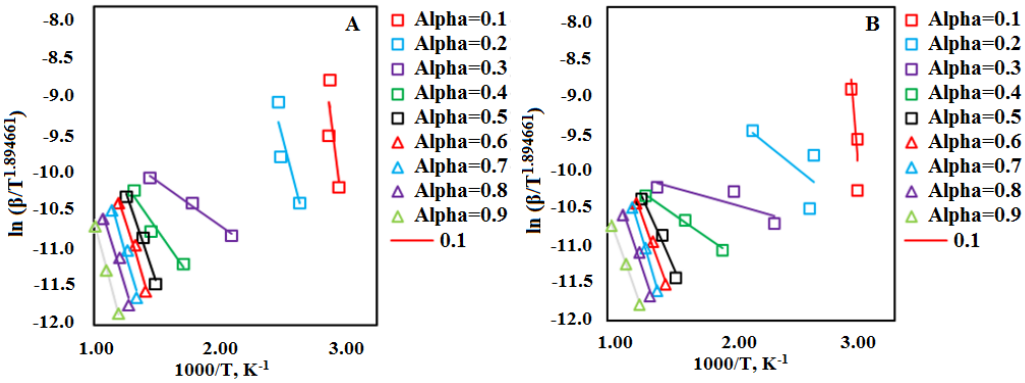

Figure 9: Linear regression lines of the Tang model at various conversion levels: [A] coke of spent 5%Co-10%Mo/AK catalyst, [B] coke of spent 5%Co-10%Mo/AB catalyst.

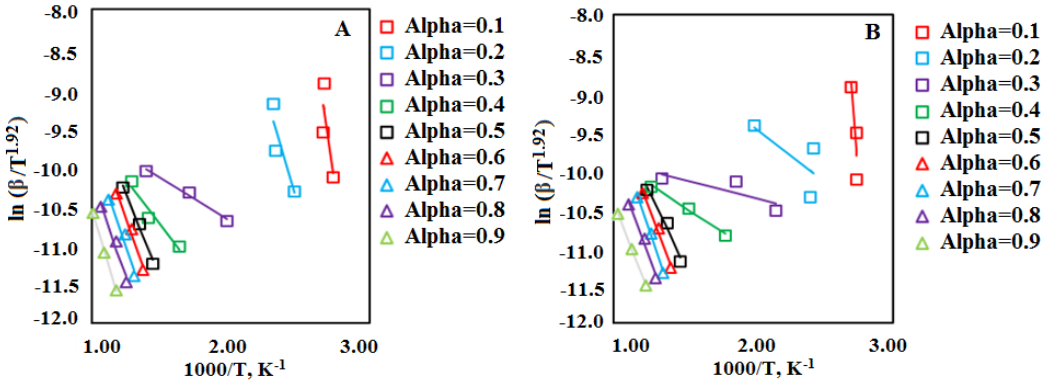

Figure 10: Linear regression lines of the Starink model at various conversion levels: [A] coke of spent 5%Co-10%Mo/AK catalyst, [B] coke of spent 5%Co-10%Mo/AB catalyst.

Consequently, the kinetic parameters, such as activation energy and pre-exponential factors, were calculated at varying conversions using model-free methods. The activation energy (E_a) was integrated from the slope of the linear equation plot. Tables 8 and 9 reveal the E_a with R^2 obtained from four model-free deactivation methods of coke over 5%Co-10%Mo/AK or AB utilized catalysts. From Table 9, the activation energy of coke over 5%Co-10%Mo/AK utilized catalyst values varies among different rate constant conversion degrees, reflecting the complexity of the multistep reactions characterizing most solid-state reactions rather than simple one-step mechanism. The linear correlation coefficients derived from fitting curves were relatively low ($R^2 < 0.95$) for the (α) value within the range of 0.1 and 0.2 in AK catalyst and 0.1-0.3 in AB catalyst, rendering these fitting curves unsuitable for activation energy calculations for the model residue. Moreover, no significant correlation was observed for transformed values below 0.1 and above 0.3 using the experimental data. This finding could be attributed to the release of soft hydrocarbon, usually in liquid form, inside the catalyst pores [40]. In the case of carbon and sulfide in the used 5%Co-10%Mo/AK catalyst, it was observed that for all (α), the average of Ea values were 57.9 kJ/mol derived from the FWO equation, 49.4 kJ/mol derived from the KAS equation, 49.9 kJ/mol derived from the Tang equation, and 49.8 kJ/mol obtained from the Starink method. These activation energies obtained from different heating rate calculations increased with the increasing heating rates.

Table 8: The iso-conversational models for coke of 5%Co-10%Mo/AK spent catalyst: comparison of calculated activation energy obtained from TGA.

Alpha (α)i	FWO		KAS		Tang		Starink	
	Eab kJmol^{-1}	R^2	Eab kJmol^{-1}	R^2	Eab kJmol^{-1}	R^2	Eab kJmol^{-1}	R^2
0.1	116778	0.6970237	116688	0.674833	116843.2	0.66604	116841.1	0.672709
0.2	59011.86	0.8244601	55106.6	0.787498	55393.59	0.78775	55341.28	0.78858
0.3	18993.51	0.999171	9993.302	0.988743	10504.13	0.990203	10384.51	0.989926
0.4	30803.97	0.9674218	21033.51	0.933827	21601.16	0.936627	21471.22	0.936066
0.5	52333.7	0.9923243	42528.23	0.985752	43125.48	0.985742	42994.91	0.985979
0.6	57770.3	0.9861443	47654.1	0.976057	48275.14	0.976235	48140.4	0.976454
0.7	59076.89	0.9692462	48400.4	0.948107	49053.39	0.949122	48911.21	0.949129
0.8	59078.72	0.9734359	47687.33	0.953311	48378.96	0.954337	48227.28	0.954318
0.9	67530.51	0.9977089	55852.73	0.996965	56570.71	0.996445	56415.17	0.996831

Table 9: The iso-conversional models for coke of 5%Co-10%Mo/AB spent catalyst: comparison of calculated activation energy obtained from TGA.

Alpha (α) i	FWO		KAS		Tang		Starink	
	Eab kJmol^{-1}	R^2	Eab kJmol^{-1}	R^2	Eab kJmol^{-1}	R^2	Eab kJmol^{-1}	R^2
0.1	215275.9	0.80135	220353.3	0.792481	220356	0.757278	220421.6405	0.781971

0.2	19346.89	0.699228	12823.42	0.481337	13200.86	0.496337	13114.11353	0.492836
0.3	13016.09	0.969446	3946.077	0.637066	4452.982	0.695617	4332.48547	0.68261
0.4	54608.08	0.999649	47910.56	0.992123	43271.95	0.993217	43740.41166	0.993022
0.5	44773.75	0.987644	37680.72	0.975032	35378.37	0.97566	35245.37225	0.975691
0.6	54107.57	0.992202	44139.95	0.985688	44748.24	0.985657	44615.50249	0.985906
0.7	61190.39	0.99833	51151.45	0.996795	51772.71	0.996283	51638.96922	0.996692
0.8	57709.24	0.985009	46819.27	0.973136	47482.04	0.973528	47337.03122	0.973668
0.9	55708.56	0.999683	43820.33	0.99896	44534.48	0.998607	44376.23142	0.998882

Consequently, the calculated activation energy calculated acquired through the KAS, Tang, and Starink methods were consistent. Conversely, higher activation energies were anticipated attributed to the slightly shifted peak temperatures (T_{peak}) associated with graphitization coke (Fig. 11) of spent 5%Co-10%Mo/AK catalyst. Additionally, the four model-free methods yielded higher activation energy. The FWO, KAS, Tang and Starink methods predicted consistent averages of activation energies of 63.9, 56.5, 56.1, and 56.0 kJ/mol, respectively. These theoretical results highlight that the lower temperature ranges (40–350 ºC) of soft coke incorporated with coke altered the model-free methods for coke of 5%Co-10%Mo/AB used catalyst and the activation energies estimation accurately.

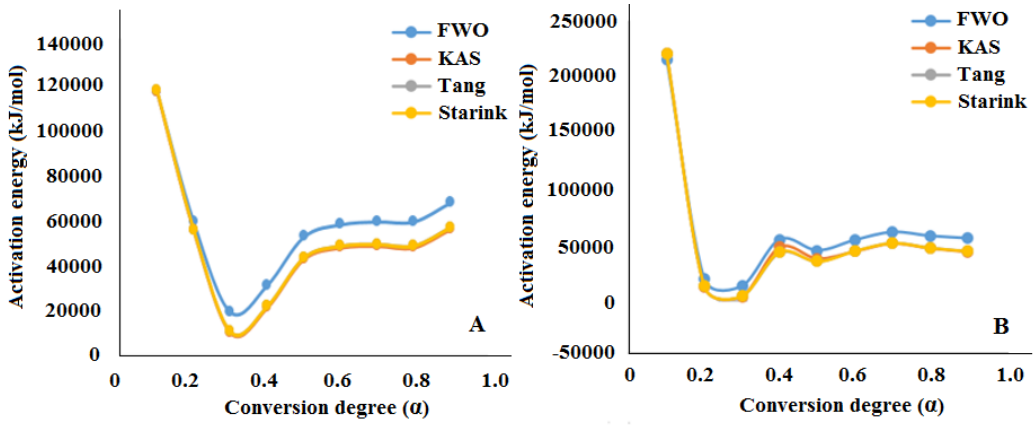

Figure 11: Obtained activation energy for conversion: [A] coke of spent 5%Co-10%Mo/AK catalyst, [B] coke of spent 5%Co-10%Mo/AB catalyst.

3.3.2 Model-Based Method

The kinetic analysis of coke oxidation over 5%Co-10%Mo/AK catalyst or coke associated with sulfide in used 5%Co-10%Mo/AB catalyst was estimated based on TGA curves, employing two independent second-order parallel reaction models. Two regions were identified: soft coke (α_1) between 100 to 300 °C and hard coke region α_2) between 300 to 850 °C, comprising a mixture of amorphous and graphitic coke. Considering the reaction model function $F3 = (1-\propto)^2$, and the presence of two peaks in the DTG curve for both catalysts, the complete coke conversion was represented by the Eq. (12) and (13):

$$\alpha = \alpha_1 + \alpha_2 + \alpha_3 \quad (12)$$

$$\frac{d\propto}{dt} = \frac{A_1}{\beta}(1-\propto_1)e^{-\frac{E_1}{RT}} + \frac{A_2}{\beta}(1-\propto_2)e^{-\frac{E_2}{RT}} + \frac{A_3}{\beta}(1-\propto_3)e^{-E_3/RT} \quad (13)$$

The apparent factors of pre-exponential (A_1, A_2, A_3) and the energies (E_1, E_2, E_3) were obtained through computational optimization of kinetic parameters to fit the experimental oxidation analysis for both utilized catalyst and three different heating rates 2.5, 5, and 10 °C/min. Fig. 12 and 13 exhibit exceptional agreement between the reaction model and the empirical findings. Table 10 lists the kinetic analysis obtained through the calculated reaction model. The Arrhenius constant and activation energy values for soft coke (α_1) and hard coke (α_2) were consistent with the literature.

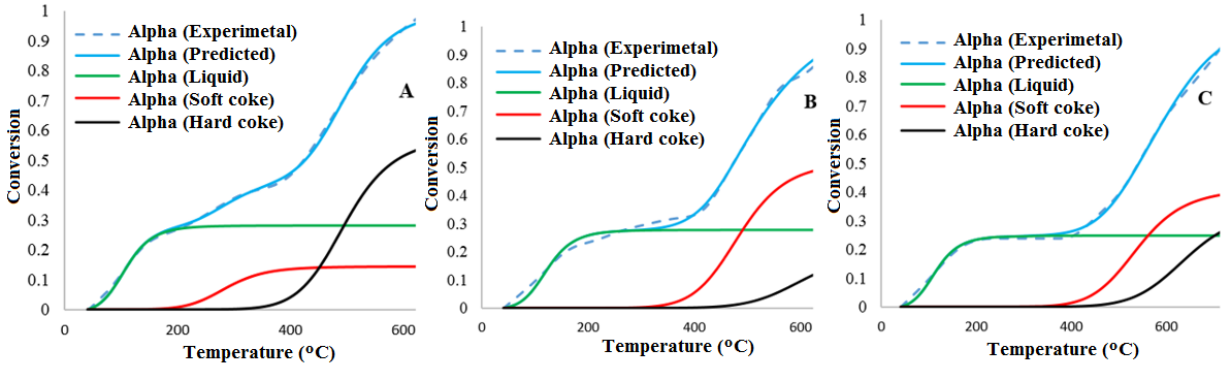

Figure 12: Comparison between actual and predicted TGA curve for coke of spent 5%Co-10%Mo/AK catalyst using multiple reaction model: [A] 2.5 °C/min, [B] 5 °C/min, [C] 10 °C/min ([1]: soft coke region, [2]: hard coke region).

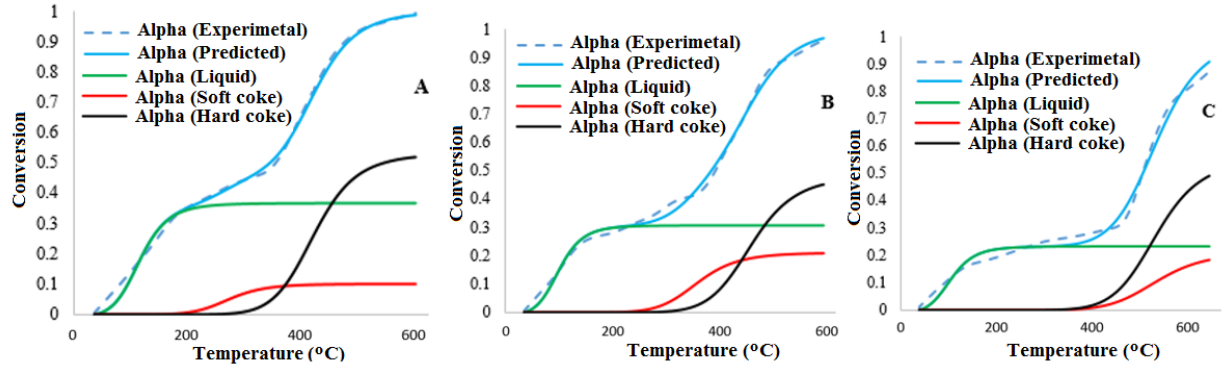

Figure 13: Comparison between actual and predicted TGA curve for coke of spent 5%Co-10%Mo/AB catalyst using multiple reaction model: [A] 2.5 °C/min, [B] 5 °C/min, [C] 10 °C/min.

Table 10: The obtained kinetic parameters using multiple reaction models.

Catalyst	E^1 kJ.mol^{-1}	E^2 kJ.mol^{-1}	E^2 kJ.mol^{-1}	Liquid wt. fraction	Soft coke fraction	Hard coke fraction	R^2
5%Co-10%Mo/AK	46.48	87.71	102.68	0.281162	0.257629	0.461208	0.991460
5%Co-10%Mo/AB	41.98	68.11	100.38	0.367911	0.101199	0.53089	0.99771

The correlation coefficient values were acceptable for both catalysts as in Z. Shakor, *et al*. [33]. The activation energy values for soft coke were 87.71 and 68.11 kJ/mol for the spent 5%Co-10%Mo/AK and 5%Co-10%Mo/AB catalysts, respectively. In contrast, the activation energy values from the hard coke region are 102.68 and 100.38 kJ/mol for spent 5%Co-10%Mo/AK and 5%Co-10%Mo/AB catalysts, respectively. The increase in the hard coke ratio in the catalyst, comprising amorphous carbon and graphitic coke, increased the corresponding activation energy.

Table 11: The obtained percentages of contaminants using multiple reaction-models.

Catalyst	Heating Rate (°C/min)	% Liquid Content	% Soft Coke Content	% Hard Coke Content	% Total Content
5%Co-10%Mo/AK	2.5	2.031	1.379	4.142	7.553
5%Co-10%Mo/AK	5	1.757	0.738	5.047	7.542
5%Co-10%Mo/AK	10	1.744	0.109	5.689	7.542
5%Co-10%Mo/AB	2.5	2.554	1.378	4.045	7.977
5%Co-10%Mo/AB	5	2.145	1.119	4.681	7.945
5%Co-10%Mo/AB	10	1.487	0.693	5.765	7.945

4. Conclusions

By analyzing the DTG data of the used catalyst, it was observed that three accumulated contents were present: liquid hydrocarbons, soft coke, and hard coke. For 5%Co-10%Mo/AK used catalyst, the peak temperatures (T_{peak}) were 517, 526 and 610 °C when the heating rates were 2.5, 5, and 10 °C/min, in the order given. While for the 5%Co-10%Mo/AB utilized catalyst, the peak temperatures (T_{peak}) were shifted lower than the previously used catalyst due to the lower temperature of amorphous carbon with graphitic coke. Activated bentonite was more receptive to coke accumulation than activated kaolin in the optimized catalyst sample. In the case of carbon and sulfide in the used 5%Co-10%Mo/AK catalyst, it was observed that for all 'α', the average of Ea values were 57.9 kJ/mol derived from the FWO equation, 49.4 kJ/mol derived from the KAS equation, 49.9 kJ/mol derived from the Tang equation, and 49.8 kJ/mol obtained from the Starink method. These activation energies obtained from different heating rate calculations increased with the increasing heating rates. The FWO, KAS, Tang and Starink methods predicted consistent averages of activation energies of 63.9, 56.5, 56.1, and 56.0 kJ/mol, respectively. These theoretical results highlight that the lower temperature ranges (40–350 °C) of soft coke incorporated with coke altered the model-free methods for coke of 5%Co-10%Mo/AB used catalyst and the activation energies estimation accurately. The kinetic analysis of coke oxidation over 5%Co-10%Mo/AK catalyst or coke associated with sulfide in spent 5%Co-10%Mo/AB catalyst was estimated based on TGA curves, employing two independent second-order parallel reaction models. The activation energy values for soft coke were 41.56 and 52.61 kJ/mol for the spent 5%Co-10%Mo/AK and 5%Co-10%Mo/AB catalysts, respectively. In contrast, the activation energy values from the hard coke region are 128.97 and 128.62 kJ/mol for utilized 5%Co-10%Mo/AK and 5%Co-10%Mo/AB catalysts, respectively. The increase in the hard coke ratio in the catalyst, comprising amorphous carbon and graphitic coke, increased the corresponding activation energy. The activation energy values for soft coke were 41.56 and 52.61 kJ/mol for the used 5%Co-10%Mo/AK and 5%Co-10%Mo/AB catalysts, respectively. In contrast, the activation energy values from the hard coke region are 128.97 and 128.62 kJ/mol for utilized 5%Co-10%Mo/AK and 5%Co-10%Mo/AB catalysts, respectively. The increase in the hard coke ratio in the catalyst, comprising amorphous carbon and graphitic coke, increased the corresponding activation energy. The mathematical model for the coke decomposition process using the model-based approach was proven more accurate than using the model-free approach. Based on the TGA test, the most suitable temperature for the regeneration process for the optimum catalyst was found to be 500 °C, and the best heating rate was 2.5 °C/min. In TGA analysis, as the heating rate increases, the removal of soft coke and liquid hydrocarbons decreases, while the removal of hard coke increases.

Conflict of Interest

The authors declare that they have no conflict of interest.

References

[1] R. Iwamoto, "Regeneration of residue hydrodesulfurization catalyst," *J. Japan Pet. Inst.*, vol. 56, no. 3, pp. 109-121, 2013.

[2] L. Mancuso and S. Arienti, "Petroleum coke (Petcoke) and refinery residues," *Integr. Gasif. Comb. Cycle (IGCC) Technol.*, vol. 2017, pp. 121-14, 2017.

[3] W. Tao, "Managing China's Petcoke Problem," *Carnegie Endowment for International Peace*, pp. 1-34, 2015.

[4] A. Saleh, "Global trends in technologies and nanomaterials for removal of sulfur organic compounds: Clean energy and green environment," *J. Mol. Liquids*, vol. 359, p. 119340, 2022.

[5] H. Nibal, M. Khudhair and A. Mohamed, "Improvement of gasoline octane number by using organic compounds," *Baghdad Sci. J.*, vol. 11, no. 2, pp. 502-508, 2014.

[6] G. Park, J. Kang, J. Park, T. Kim, G. Kwak, and S. Kim, "Effect of acid modification of ZSM-5 catalyst on performance and coke formation for methanol-to-hydrocarbon reaction," *Mol. Catal.*, vol. 531, p. 112702, 2022.

[7] S. Kwao, S. Vedachalam, K. Dalai and J. Adjaye, "Review of current advances in hydrotreating catalyst support," *J. Ind. Eng. Chem.*, vol. 2024.

[8] H. Topsøe, B. Clausen, R. Candia, C. Wivel, and S. Mørup, "In situ Mössbauer emission spectroscopy studies of unsupported and supported sulfided Co Mo hydrodesulfurization catalysts: Evidence for and nature of a Co Mo S phase," *J. Catal.*, vol. 68, pp. 433-452, 1981.

[9] Y. Yoshimura, T. Sato, H. Shimada, N. Matsubayashi, M. Imamura, A. Nishijima, S. Yoshitomi, T. Kameoka, and H. Yanase, "Oxidative regeneration of spent molybdate and tungstate hydrotreating catalysts," *Energy Fuels*, vol. 8, pp. 435-445, 1994.

[10] G. Murali Dhar, N. Srinivas, M. Rana, M. Kumar and K. Maity, "Mixed oxide supported hydrodesulfurization catalysts—a review," *Catal. Today*, vol. 86, no. 1-4, pp. 45-60, 2003.

[11] I. Mochida and H. Choi, "An overview of hydrodesulfurization and hydrodenitrogenation," *J. Japan Pet. Inst.*, vol. 47, no. 3, pp. 145-163, 2004.

[12] K. Bej, K. Maity, and T. Turaga, "Search for an efficient 4,6-DMDBT hydrodesulfurization catalyst: A review of recent studies," *Energy Fuels*, vol. 18, no. 5, pp. 1227-1237, 2004.

[13] C. Song, "An overview of new approaches to deep desulfurization for ultra-clean gasoline, diesel fuel and jet fuel," *Catal. Today*, vol. 86, no. 1-4, pp. 211-263, 2003.

[14] N. Ipatieff, "On the action of sulfuric acid on the acetylene hydrocarbon," *Journal of the Russian Physical-Chemical Society*, vol. 38, p. 75, 1906.

[15] F. Bergius, "Chemical reactions under high pressure, Nobel lecture," *Nobel Prize website*, 1932. [Online]. Available: http://nobelprize.org/nobel-prizes/chemistry/laureates/1931/bergius-lecture.html.

[16] P. Sudarsanam, B. Hillary, K. Deepa, H. Amin, B. Mallesham, B. Reddy, and K. Bhargava, "Highly efficient cerium dioxide nanocube-based catalysts for low temperature diesel soot oxidation: The cooperative effect of cerium- and cobalt-oxides," *Catal. Sci. Technol.*, vol. 5, pp. 3496-3500, 2015.

[17] T. Fujimori and M. Takaoka, "Direct chlorination of carbon by copper chloride in a thermal process," *Environ. Sci. Technol.*, vol. 43, no. 7, pp. 2241-2246, 2009.

[18] X. Zou, et al., "Catalytic effects of metal chlorides on the pyrolysis of lignite," *Energy Fuels*, vol. 21, no. 2, pp. 619-624, 2007.

[19] Q. Song, B. He, Q. Yao, Z. Meng, and C. Chen, "Influence of diffusion on thermogravimetric analysis of carbon black oxidation," *Energy Fuels*, vol. 20, pp. 1895-1900, 2016.

[20] S. Salvador, J. Commandre, and B. Stanmore, "Reaction rates for the oxidation of highly sulphurised petroleum cokes: The influence of thermogravimetric conditions and some coke properties," *Fuel*, vol. 82, pp. 715-720, 2003.

[21] B. Govindan, S. Chandra, B. Jakka, K. Radhakrishnan, K. Tiwari, T. Sudhakar, et al., "Investigation on kinetic parameters of combustion and oxy-combustion of calcined pet coke employing thermogravimetric analysis coupled to artificial neural network modeling," *Energy Fuels*, vol. 32, pp. 3995-4007, 2018.

[22] L. Hu, Y. Zhang, D. Chen, J. Fang, M. Zhang, Y. Wu, H. Zhang, Z. Li, and J. Lyu, "Experimental study on the combustion and NOx emission characteristics of a bituminous coal blended with semi-coke," *Appl. Therm. Eng.*, vol. 160, p. 113993, 2019.

[23] H. Yao, B. He, G. Ding, W. Tong, and Y. Kuang, "Thermogravimetric analyses of oxy-fuel co-combustion of semicoke and bituminous coal," *Appl. Therm. Eng.*, vol. 156, pp. 708-721, 2019.

[24] K. Jayaraman, V. Kok, and I. Gokalp, "Thermogravimetric and mass spectrometric (TG-MS) analysis and kinetics of coal-biomass blends," *Renewable Energy*, vol. 101, pp. 293-300, 2017.

[25] J. Nisar et al., "Fuel production from waste polystyrene via pyrolysis: Kinetics and products distribution," *Waste Manag.*, vol. 88, pp. 236-247, 2019. doi: 10.1016/j.wasman.2019.

[26] A. Brems, J. Baeyens, J. Beerlandt, and R. Dewil, "Thermogravimetric pyrolysis of waste polyethylene-terephthalate and polystyrene: A critical assessment of kinetics modelling," *Resour. Conserv. Recycl.*, vol. 55, no. 8, pp. 772-781, 2011. doi: 10.1016/j.resconrec.2011.

[27] A. Singh, T. Sharma, and P. Kishore, "Thermal degradation kinetics and reaction models of 1,3,5-triamino-2,4,6-trinitrobenzene-based plastic-bonded explosives containing fluoropolymer matrices," *J. Therm. Anal. Calorim.*, vol. 129, no. 3, pp. 1403-1414, 2017. doi: 10.1007/s10973-017-6335-z.

[28] X. Kai, T. Yang, S. Shen, and R. Li, "TG-FTIR-MS study of synergistic effects during co-pyrolysis of corn stalk and high-density polyethylene (HDPE)," *Energy Convers. Manag.*, vol. 181, pp. 202-213, 2019. doi: 10.1016/j.enconman.2018.

[29] S. Yousef, J. Eimontas, N. Striugas, K. Zakarauskas, M. Praspaliauskas, and M. A. Abdelnaby, "Pyrolysis kinetic behavior and TG-FTIR-GC–MS analysis of metallised food packaging plastics," *Fuel*, vol. 282, p. 118737, June 2020. doi: 10.1016/j.fuel.2020.118737.

[30] M. Khosravinezhad and M. Kazemi, "Study on kinetics of thermal degradation of Polymethyl Methacrylate / Cyclic Olefin Copolymer blend," *May 2021*. doi: 10.20944/preprints202105.0587.v1.

[31] R. Pan, J. V. F. Duque, and G. Debenest, "Investigating waste plastic pyrolysis kinetic parameters by genetic algorithm coupled with thermogravimetric analysis," *Waste Biomass Valorization*, vol. 12, no. 5, pp. 2623-2637, 2021. doi: 10.1007/s12649-020-01181-4.

[32] A. Lechleitner, T. Schubert, W. Hofer, and M. Lehner, "Lumped kinetic modeling of polypropylene and polyethylene co-pyrolysis in tubular reactors," *Processes*, vol. 9, no. 1, pp. 1-15, 2021. doi: 10.3390/pr9010034.

[33] Z. Hussein, Z. Shakor, M. Alzuhairi and F. Al-Sheikh, "Kinetic and thermodynamic study of the pyrolysis of plastic waste," *Environ. Processes*, vol. 10, no. 2, p. 27, 2023.

[34] P. Nasution, J. Jung, K. Oh and L. Koh, "Coke combustion kinetics of spent Pt-Sn/Al_2O_3 catalysts in propane dehydrogenation," *Korean J. Chem. Eng.*, vol. 37, pp. 1490-1497, 2020.

[35] F. Hu, B. Xiong, X. Liu, X. Huang, Y. Li and Z. Liu, "Optimized TGA-based experimental method for studying intrinsic kinetics of coal char oxidation under moderate or intense low-oxygen dilution oxy-fuel conditions," *Energy*, vol. 265, p. 126318, 2023.

[36] G. Jiang and L. Wei, "Analysis of pyrolysis kinetic model for processing of thermogravimetric analysis data," *Phase Chang. Mater. Their Appl.*, vol. 10, 2018.

[37] V. Leroy, D. Cancellieri, E. Leoni and L. Rossi, "Kinetic study of forest fuels by TGA: Model-free kinetic approach for the prediction of phenomena," *Thermochim. Acta*, vol. 497, no. 1-2, pp. 1-6, 2010.

[38] Z. Alhulaybi and I. Dubdub, "Comprehensive kinetic study of PET pyrolysis using TGA," *Polymers*, vol. 15, no. 14, p. 3010, 2023.

[39] I. Eslami and D. Ching, "Effect of novel swirl distributor plate on hydrodynamics of fluidized bed gasifier," *Int. J. Eng.*, vol. 32, no. 10, pp. 1358-1365, 2019.

[40] Z. Shakor, A. Alasseel, and E. Al-Shafei, "The structure of deposited coke on hydrocracking and reforming catalysts: Coke deactivation and kinetics", *The Canadian Journal of Chemical Engineering, 2024.*

[41] Y. Zhitong, et al, "Kinetic studies on the pyrolysis of plastic waste using a combination of model-fitting and model-free methods." *Waste Management & Research* 38.1-suppl, 77-85, 2020.

[42] Z. Zhang, J. Peng, W. Qu, L. Zhang, Z. Zhang, W. Li and R. Wan, "Regeneration of high-performance activated carbon from spent catalyst: Optimization using response surface methodology," *J. Taiwan Inst. Chem. Eng.*, vol. 40, no. 5, pp. 541-548, 2009.

[43] M. Heydari, M. Rahman, and R. Gupta, "Kinetic study and thermal decomposition behavior of lignite coal," *Int. J. Chem. Eng.*, vol. 2015, article ID 481739, 2015.

[44] X. Yongjiang, X. Huaqing, W. Hongyan, L. Zhiping and F. Chaohe, "Kinetics of isothermal and non-isothermal pyrolysis of oil shale," *Oil Shale*, vol. 28, no. 3, 2011.

[45] S. Sobek and S. Werle, "Kinetic modelling of waste wood devolatilization during pyrolysis based on thermogravimetric data and solar pyrolysis reactor performance," *Fuel*, vol. 261, p. 116459, 2020.

[46] C. Doyle, "Series approximations to the equation of thermogravimetric data," *Nature*, vol. 207, no. 4994, pp. 290-291, 1965.

[47] S. Vyazovkin et al., "ICTAC Kinetics Committee recommendations for performing kinetic computations on thermal analysis data," *Thermochim. Acta*, vol. 520, no. 1-2, pp. 1-19, 2011.

[48] W. Tang, Y. Liu, H. Zhang and C. Wang, "New approximate formula for Arrhenius temperature integral," *Thermochim. Acta*, vol. 408, no. 1-2, pp. 39-43, 2003.

[49] J. Starink, "The determination of activation energy from linear heating rate experiments: A comparison of the accuracy of isoconversion methods," *Thermochim. Acta*, vol. 404, no. 1-2, pp. 163-176, 2003.

[50] A. Flores, J. Juan, et al., "Analysis of pyrolysis kinetic parameters based on various mathematical models for more than twenty different biomasses: a review", *Energies* 15.18, 6524, 2022.

[51] X. Zhilin, et al., "Analysis of coal spontaneous combustion by thermodynamic methods", *Combustion Science and Technology* 193.13: 2305-2330, 2021.

[52] Z. Abdulhamid, and I. Dubdub, "Kinetics Study of PVA Polymer by Model-Free and Model-Fitting Methods Using TGA", *Polymers* 16.5: 629, 2024.

[53] F. Olivier, R. Lemaire, and A. Bensakhria, "Thermogravimetric analysis and kinetic modeling of the pyrolysis of different biomass types by means of model-fitting, model-free and network modeling approaches", *Journal of Thermal Analysis and Calorimetry*, 1-23, 2024.

[54] N. Arenas, V. Navarro, and D. Martínez, "Pyrolysis kinetics of biomass wastes using isoconversional methods and the distributed activation energy model," *Bioresour. Technol*., vol. 288, p. 121485, 2019.

[55] M. Ameen, T. Azizan, A. Ramli, S. Yusup and M. Yasir, "Physicochemical properties of Ni-Mo/γ-Al_2O_3 catalysts synthesized via sonochemical method," *Procedia Eng*., vol. 148, pp. 64-71, 2016.

[56] A. Hart, M. Adam, P. Robinson, P. Rigby and J. Wood, "Hydrogenation and dehydrogenation of tetralin and naphthalene to explore heavy oil upgrading using NiMo/Al_2O_3 and CoMo/Al_2O_3 catalysts heated with steel balls via induction," *Catalysts*, vol. 10, no. 5, p. 497, 2020.

[57] V. Baldovino-Medrano, A. Giraldo, and A. Centeno, "The functionalities of Pt/γ-Al_2O_3 catalysts in simultaneous HDS and HDA reactions," *Fuel*, vol. 87, no. 10-11, pp. 1917-1926, 2008.

[58] H. Hasanudin, K. Wijaya, and B. Santoso, "Preparation and catalytic activity for isopropyl benzene cracking of Co, Mo and Co/Mo- Al_2O_3-pillared montmorillonite catalysts", *Indonesian Journal of Chemistry* 9.2, 189-194, 2009.